

Catalysis Science & Technology

Accepted Manuscript



This is an *Accepted Manuscript*, which has been through the Royal Society of Chemistry peer review process and has been accepted for publication.

Accepted Manuscripts are published online shortly after acceptance, before technical editing, formatting and proof reading. Using this free service, authors can make their results available to the community, in citable form, before we publish the edited article. We will replace this *Accepted Manuscript* with the edited and formatted *Advance Article* as soon as it is available.

You can find more information about *Accepted Manuscripts* in the [Information for Authors](#).

Please note that technical editing may introduce minor changes to the text and/or graphics, which may alter content. The journal's standard [Terms & Conditions](#) and the [Ethical guidelines](#) still apply. In no event shall the Royal Society of Chemistry be held responsible for any errors or omissions in this *Accepted Manuscript* or any consequences arising from the use of any information it contains.

ARTICLE

Ag-Pd and CuO-Pd Nanoparticles in a Hydroxyl-group Functionalized Ionic Liquid: Synthesis, Characterization and Catalytic Performance

Cite this: DOI: 10.1039/x0xx00000x

Bin Zhang^a, Yuan Yuan^a, Karine Philippot^{b,c}, Ning Yan^{*a}

Received 00th January 2012,

Accepted 00th January 2012

DOI: 10.1039/x0xx00000x

www.rsc.org/

Heteronuclear Ag-Pd and CuO-Pd nanoparticles with controllable Ag:Pd or Cu:Pd ratio were easily synthesized through thermal decomposition of their acetate salts in a functionalized ionic liquid [C₂OHmim][NTf₂]. The structural and electronic properties of these particles were characterized with ICP-OES, TEM, XRD and XPS techniques. The Ag-Pd nanoparticles have a silver enriched core covered by a Pd enriched shell. The addition of Ag clearly enhanced the catalytic activity of Pd in the hydrogenation of -NO₂, and -C=C- functionalities. Interestingly, in the CuO-Pd nanoparticles, the Pd tends to stay in the inner part of the particle, leaving the outer layer rich in CuO, which exhibit less activity than Pd NPs.

Introduction

Metal nanoparticles (NPs) that are composed of two different metal elements, namely bimetallic NPs, have long been receiving considerable attention due to their distinct physicochemical properties compared to monometallic counterparts. Indeed, new properties can be derived from electronic and steric interaction between the two metal components.¹⁻⁴ In catalysis this can lead to improvement of performance both in terms of activity and selectivity. There are generally three types of structures for bimetallic NPs,^{5,6} including nano-alloy,^{7,8} heterodimer⁹ and core-shell (or partial core-shell)¹⁰ structures. The core-shell configuration is featured by one metal constituting (or dominating) the core of particles whereas the second one is taking up (or enriching in) the outer layer.¹¹ This peculiar structure sometimes endows NPs an outstanding catalytic activity over those of alloyed NPs or heterodimers.¹²⁻¹⁵ For instance, core-shell Rh-Pt NPs outperform equivalent Pt_{1-x}Rh_x alloys and monometallic mixtures.¹⁶ Currently, a variety of bimetallic NPs with core-shell structures have been investigated, such as Au-Pd¹⁷⁻¹⁹, Au-Ag^{20,21}, Pt-Rh^{2,16,22}, Pt-Ru²³⁻²⁵, Pt-Pd²⁶⁻²⁸, and Ni-M NPs (M=Au, Rh, Ru, Pd)^{29,30}.

For stabilization of metal NPs in liquid phase, proper solvents and/or stabilizers are often employed to prevent them from

agglomeration.⁴ Among various solvents, ionic liquids (ILs) are attractive since they can act as both stabilizer for NPs and reaction medium.³¹⁻³⁶ Furthermore, the properties of ILs can be tailored by modifying their chemical structure through incorporation of different functional groups³⁷⁻³⁹, such as hydroxyl,⁴⁰⁻⁴² nitrile,^{43,44} thiol^{45,46} or carboxyl^{47,48} groups onto the cation or the anion. These functional groups may interact with NP metallic surface and further provide higher stability to metal NPs as well as influence their performance in catalytic reactions.^{40,46,47,49-52} Recently, a number of bimetallic NPs synthesized in ILs have been reported. Au-M (M=Pd, Ag, Pt) NPs were investigated intensively with either non-functionalized and functionalized ILs or ionic liquid composites.⁵³⁻⁵⁷ Besides, Pt-M (M=Co, Ru, Pd)⁵⁸⁻⁶⁰, Ru-Cu⁶¹ and Pd-Ni⁶² bimetallic NPs-ionic liquid systems were also studied. Previously we prepared core-shell Au-Pd bimetallic NPs displaying a Pd-enriched surface around an Au-core, in 1-ethyl-3-methylimidazoliumbis-(trifluoromethylsulfonyl) imide ([C₂OHmim][NTf₂]).⁶³ This IL was selected after screening a series of different ILs to provide the NPs with the highest stability as well as well-controlled size.⁶⁴ In hydroxyl-functionalized imidazolium based IL the hydroxyl group may both accelerate the formation of NPs and help their protection from oxidation. The so-obtained Au-Pd NPs exhibited higher selectivity for the dehalogenation of aryl halides than pure Pd

NPs, while pure Au NPs were inactive. The enhanced selectivity of Au-Pd bimetallic NPs was attributed to the enrichment of Pd on the surface and the charge transfer from Pd to Au. It is worth noting that the synthetic method applied for synthesizing these Au-Pd NPs, i.e., thermal-decomposition of the two metal acetates under vacuum,⁶⁴ is simpler compared with other approaches, such as decomposition through thermal treating with H₂,^{65,66} reduction with chemical or electrical agent,^{38,67} bombardment of large particles through irradiation⁶⁸ or transfer of pre-synthesized NPs into ionic liquids,⁶⁹ for example.

Motivated by the effectiveness and the simplicity of the thermal-decomposition under vacuum method for Au-Pd NPs, we envisaged to extend this methodology to the synthesis of other bimetallic NPs in ILs. Considering that both Pd and Au are noble metals, it is economically attractive to replace the core metal with another metal having higher natural abundance and much cheaper price.^{70,71} For this purpose, Ag and Cu, staying in the same group as Au in the elemental table, appeared as ideal. So far, only limited researches on Ag-Pd and Cu-Pd bimetallic systems in ILs have been reported. Tai et al. prepared a series of Ag-Pd alloys (larger than 100 nm) *via* electrodeposition.⁷² Safavi et al. obtained Ag-Pd nanoalloys through microwave-assisted decomposition and used them in electrocatalysis.^{73,74} Thus, it is challenging to synthesize Ag-Pd and Cu-Pd bimetallic NPs of smaller size *via* simple methods and to study their catalytic properties. In this context, we report here the synthesis of Ag-Pd and CuO-Pd NPs by thermal co-decomposition of acetate salts under vacuum in [C₂OHmim][NTf₂]. The catalytic performance of the so-obtained Ag-Pd and CuO-Pd NPs was also studied in detail, namely in hydrogenation and hydrodehalogenation reactions of model substrates.

Results and discussion

Synthesis of Ag-Pd NPs in [C₂OHmim][NTf₂]

A series of three bimetallic Ag-Pd NPs was synthesized through thermal decomposition (393 K, 2 h) under vacuum of the two metal acetates in [C₂OHmim][NTf₂]. Monometallic Pd and Ag NPs were also prepared in the same manner, as control samples. After two hours' thermal decomposition, the reaction medium formed a stable colloidal solution, making it possible to conduct catalytic reactions without further treatment. The IL thus functions as both the solvent and the stabilizer. According to the ratio of the two starting metal precursors, the resulting NPs are denoted as Pd, Ag_{0.2}Pd_{0.8}, Ag_{0.5}Pd_{0.5}, Ag_{0.8}Pd_{0.2} and Ag respectively.

Characterization of Ag-Pd bimetallic NPs

The as-prepared Ag-Pd NPs were first characterized by Transmission Electron Microscopy (TEM). The representative images and size distributions obtained for Ag, Ag-Pd and Pd NPs are presented in Figure 1. Most of the Ag-Pd NPs are spherical and have narrow size distributions, with average

diameters between 3.4 and 3.7 nm, showing that the incorporation of Ag to Pd does not change the size of the NPs significantly. Ag-Pd bimetallic NPs with similar size and morphology were previously obtained through an ion-exchange method on ultrathin TiO₂-gel films,⁷⁵ and through supporting two nitrates on reduced graphene oxide.⁷⁶ Compared with these previous methods, the NPs described here are more uniform and monodispersed in size, indicating that the functionalized ionic liquid may play an important role. To obtain a thorough understanding of the structural features of the Ag-Pd NPs, ICP-OES, XPS, XRD analyses were subsequently conducted.

The metal composition of the Ag-Pd NPs was calculated from the ICP-OES analysis (see Table 1). The atomic composition appeared close to the ratio of the two metal precursors introduced for the NP synthesis. This result implies that the Ag/Pd ratio can be easily tuned by adjusting the ratio of precursors during preparation.

XRD is an efficient tool to identify the structure of NPs, especially for bimetallic NPs.^{73,77,78} The XRD spectra of all NP samples are compiled in Figure 2. For monometallic Pd NPs, the observed intense peaks at 40°, 47°, 68° and 81° are representing the (111), (200), (220), and (311) Bragg reflections of Pd cubic (fcc) crystalline, respectively, which is in excellent agreement with literature data. For Ag NPs, these four peaks are centred at 38°, 44°, 64° and 77°. Interestingly, in the XRD patterns of all the Ag-Pd bimetallic NPs, the diffraction peaks are located at 38°, 44°, 64°, 77° and 82°, matching exactly the reflections of metallic Ag in (111), (200), (220), (311) and (222) planes. No other peaks were observed. This suggests that the Ag-Pd NPs do not form alloy structures and only the silver atoms constitute the crystalline structure. Previous XRD studies on Ag-Pd NPs from literature^{76,79-81} show that the observed diffraction peaks are between those of monometallic Ag and Pd, suggesting the formation of alloy structures. The Ag-Pd NPs we here describe appear thus structurally different from those in previous reports (*vide infra*). The crystalline size of the NPs was also calculated using peak broadening profile of (111) peak at 38° and 40° respectively through the Sherrer equation. The calculated values (ca. 3-5 nm) matches the TEM results, further confirming that the particle sizes of the Ag-Pd NPs prepared in [C₂OHmim][NTf₂] are very small.

XPS was employed to investigate the elemental composition and electronic state of the NP surface. The XPS spectra of Pd 3d and Ag 3d electron for the whole series of NPs are shown in Figure 3. The near-surface elemental ratio was calculated based on the fitted curves of XPS data, revealing that Pd has a higher tendency to locate near the surface than Ag (Table 1). From XRD and XPS results, it is highly plausible that the Ag-Pd NPs adopt a core (Ag) - shell (Pd) structure, as similarly observed in a thermodynamic study of the surface segregation of Ag₃Pd under environment rich in oxygen.⁸² In this published study, DFT results showed that the segregation energy of AgPd alloy decreases with the increase of Ag percentage of topmost layer, while the oxygen binding energy increases with more Pd on the surface.⁸² Therefore, the formation of Pd enriched shell in

vacuum suggests that the hydroxyl functionalized ionic liquid [C₂OHmim][NTf₂] may play a dominant role in controlling the structure of the Ag-Pd NPs.

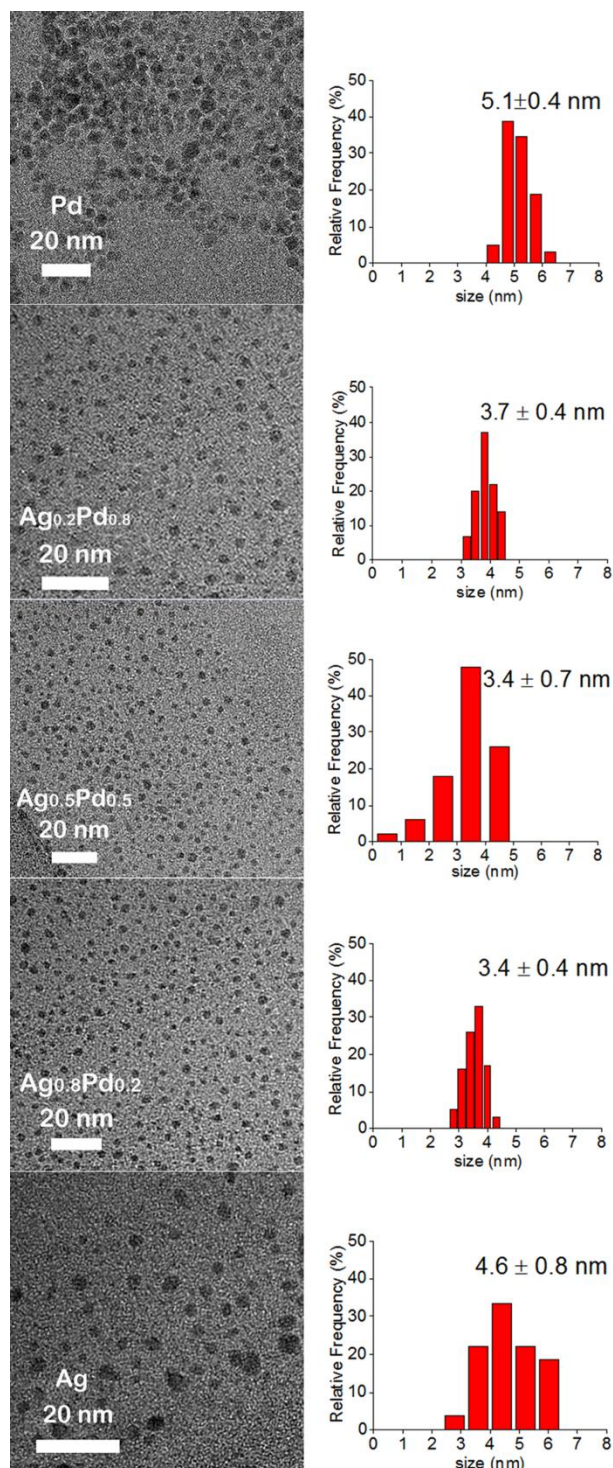


Figure 1. TEM images and corresponding size distributions of Pd NPs, Ag-Pd NPs and Ag NPs synthesized in [C₂OHmim][NTf₂].

A close inspection on the Pd 3d XPS spectra reveals that the peaks ranging from 335.1–335.4 eV and 341.1–341.4 eV can be attributed to the 3d_{5/2} and 3d_{3/2} spin-orbit states of zero-valent

Table 1. Elemental composition of Ag-Pd NPs calculated from ICP analysis and the near-surface composition calculated from XPS analysis.

NPs	Ag/Pd ratio (ICP)	Ag/Pd ratio (XPS)
Ag-Pd (4:1) ^a	3.06:1	1.2:1
Ag-Pd (1:1)	0.92:1	0.48:1
Ag-Pd (0.25:1)	0.26:1	0.22:1

[a] This ratio corresponds to the initial molar amounts of the two acetate precursors.

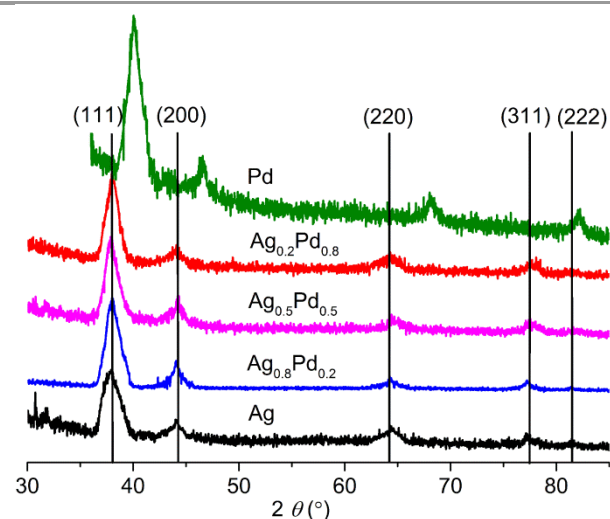


Figure 2. X-ray diffraction patterns of the Ag, Ag-Pd and Pd NPs. The predicted diffraction peaks for Ag metal and Pd metal are indicated. From top to bottom: Pd, Ag_{0.2}Pd_{0.8}, Ag_{0.5}Pd_{0.5}, Ag_{0.8}Pd_{0.2}, and Ag NPs.

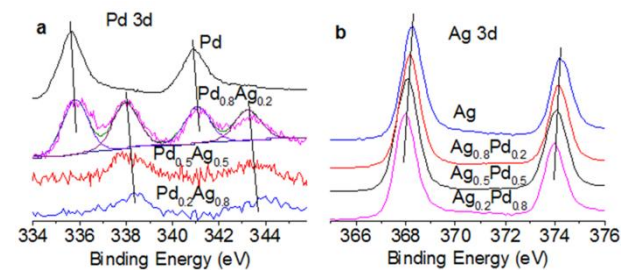


Figure 3. XPS spectra of Pd 3d peak (a) and Ag 3d peak (b) for Ag-Pd NPs

Pd, whereas peaks ranging from 338.0–338.5 eV and 343.7–344.2 eV correspond to the states of Pd (II). It is obvious that when the concentration of Ag increases, Pd species tends to stay at a higher valence state. Furthermore, the binding energy increases with increasing Ag content. Ag_{0.2}Pd_{0.8} NPs contains both Pd(0) and Pd(II) with a ratio of 1:1.2 for near surface atoms, according to the XPS curve fitting. From the positions of Ag 3d_{5/2} (368.0–368.5 eV) and 3d_{3/2} (374.0–374.5 eV) peaks in the XPS spectra, the valence state of Ag in Ag-Pd NPs is always zero, regardless of the Pd content. The binding energies of Ag 3d electrons tend to decrease with increasing Pd in the NPs, thus Ag becoming electronically negative. This reveals that Pd donates electrons to Ag in the Ag-Pd NPs, resulting in negatively charged Ag and positively charged Pd. Another reason accounting for the positively charged Pd may be that the Pd preferentially locates at the outer shell and therefore can

have more interaction with electronegative elements such as oxygen from the hydroxyl-functionalized IL.

Application of Ag-Pd NPs in catalysis

Four catalytic reactions were conducted to evaluate the catalytic performances of the series of as-prepared Ag-Pd NPs in [C₂OHmim][NTf₂]. These reactions include: hydrogenation of 4-nitrophenol, nitrobenzene, and styrene, and hydrodehalogenation of 4-bromotoluene. As a control, the catalytic performances of single component Ag and Pd nanocatalysts were also evaluated.

The hydrogenation of 4-nitrophenol over Pd, Ag-Pd and Ag NPs was carried out in the presence of H₂ (3 MPa) at 353 K for 2 h. The results are compiled in Table 2 (Entry 1-5, activity is calculated based on the Pd content determined by ICP. The results indicate that the Ag-Pd bimetallic NPs are significantly more active in hydrogenation of 4-nitrophenol compared with the monometallic Pd and Ag NPs. Indeed, Ag NPs were observed inactive whereas Pd NPs exhibited very low activity (0.7 h⁻¹) under the conditions applied. Incorporating 20% Ag into Pd enabled improvement of the activity to one order of magnitude higher (4.8 h⁻¹), and the activity kept increasing when the Ag content was further increased. The activity reached 55 h⁻¹ for Pd_{0.2}Ag_{0.8} NPs, ca. 80 times more active than single component Pd NPs. Aminophenol is the only product, suggesting this is a highly selective system for nitro group reduction without further hydrogenation.

The hydrogenation of nitrobenzene is known to be easier than that of 4-nitrophenol⁸³⁻⁸⁵, due to the fact that -OH group affects the electronic state of the substrate. As such, the hydrogenation of nitrobenzene was carried out under milder reaction conditions (2 MPa H₂, 333 K, see Table 3, Entry 1-5). Noteworthy, promotional effect of Ag to Pd was observed in Ag-Pd NPs until a certain point. Indeed, the activity of Pd did not exhibit a monotonic trend with increasing content of Ag. Instead, Ag_{0.5}Pd_{0.5} NPs appeared to be the most effective nanocatalyst and further increasing of Ag to 80 % induced undesired side reactions. Interestingly, the selectivity for aminocyclohexane was enhanced over Ag enriched catalysts, especially Ag_{0.8}Pd_{0.2}. Considering that electrons were transferred from Pd to Ag, positively charged Pd surface species may act as Lewis acid, which can activate benzene ring for hydrogenation.⁸⁶

Hydrogenation of styrene also revealed the superior catalytic activity of Ag-Pd NPs (Table 4, Entry 1-5). Since both Pd and Ag can catalyse the reaction to a similar degree, activity was calculated based on the total amount of catalysts. The activity of Ag_{0.5}Pd_{0.5} NPs increased ca. 3 times compared with those of Ag and Pd NPs under the same reaction conditions. In all the cases, hydrogenation of benzene ring was not observed in the applied reaction conditions, providing 100% selectivity into ethylbenzene.

Considering that all the NPs in the series have similar mean particle size, the difference observed in catalytic activity cannot be attributed to size effect. Thus, the increase in catalytic activity with increasing Ag content in the bimetallic Ag-Pd NPs

may be attributed to both the enrichment of Pd on the surface and the electronic modifications of the Pd atoms induced by the presence of electronegative Ag atoms. The positive charged Pd atoms could facilitate the adsorption of the substrates on the metallic surface which would favour higher conversion.

Table 2. Hydrogenation of 4-nitrophenol catalysed by Ag, Pd, CuO, Ag-Pd and CuO-Pd NPs in [C₂OHmim][NTf₂].^a

Entry	NPs	Conversion [%]	Activity ^b [h ⁻¹]	Selectivity for 4-aminophenol [%]	Selectivity for 4-aminocyclohexanol [%]
1	Pd	1.4	1.2	100	0
2	Ag _{0.2} Pd _{0.8}	7.8	4.8	100	0
3	Ag _{0.5} Pd _{0.5}	23	23	100	0
4	Ag _{0.8} Pd _{0.2}	11	30	100	0
5	Ag	0	-	-	-
6	(CuO) _{0.2} Pd _{0.8}	1.1	0.8	100	0
7	(CuO) _{0.5} Pd _{0.5}	0.8	0.8	100	0
8	(CuO) _{0.8} Pd _{0.2}	0.3	0.7	100	0
9	CuO/Cu ₂ O	0	-	-	-

[a] Reaction conditions: 4-nitrophenol (0.5 mmol), NP-IL (0.05 mL), IL (0.45 mL), K₂CO₃ (0.05 g) H₂ (3 MPa), 353 K, 2 h (IL = [C₂OHmim][NTf₂]). [b] activity = moles of converted substrate/moles of Pd

Table 3. Hydrogenation of nitrobenzene catalysed by Ag, Pd, CuO, Ag-Pd and CuO-Pd NPs in [C₂OHmim][NTf₂].^a

Entry	NPs	Conversion [%]	Activity ^b [h ⁻¹]	Selectivity for aniline [%]	Selectivity for aminocyclohexane [%]
1	Pd	52	52	99.7	0.3
2	Ag _{0.2} Pd _{0.8}	67	84	99.8	0.2
3	Ag _{0.5} Pd _{0.5}	77	154	99.7	0.3
4	Ag _{0.8} Pd _{0.2}	25	100	89.1	10.9
5	Ag	9	-	92.4	7.6
6	(CuO) _{0.2} Pd _{0.8}	13	9.5	100	0
7	(CuO) _{0.5} Pd _{0.5}	5.1	5.1	100	0
8	(CuO) _{0.8} Pd _{0.2}	3.4	7.8	100	0
9	CuO/Cu ₂ O	0.4	-	100	0

[a] Reaction conditions: nitrobenzene (1 mmol), NP-IL (0.05 mL), IL (0.45 mL), H₂ (2 MPa), 333 K, 2 h (IL = [C₂OHmim][NTf₂]). [b] activity = moles of converted substrate/moles of Pd.

Previously, Au-Pd bimetallic NPs were found to be much more effective than Au and Pd NP counterparts in hydrodehalogenation reactions.⁶³ Thus, dehalogenation of 4-bromotoluene was also studied over Ag, Pd and Ag-Pd NPs (Table 5, Entry 1-5). Ag was inactive for the reaction but the addition of Ag enhanced the catalytic performance of Pd. However, the enhancement in activity is not as strong as in the case of Au-Pd NPs.⁶³ Two reasons may account for this: a) the electronic interaction between Ag-Pd is different from that of Au-Pd, resulting in different catalytic properties; b) although the NPs have a Pd-enriched shell, a small percentage of Ag atoms may still exist on the surface and bind with Br⁻, which could poison the catalysts.

Table 4. Hydrogenation of styrene catalysed by Ag, Pd, CuO, Ag-Pd and CuO-Pd NPs in [C₂OHmim][NTf₂].^a

Entry	NPs	Conversion [%]	Activity [h ⁻¹]	Selectivity for ethylbenzene [%]	Selectivity for ethylcyclohexane [%]
1	Pd	27	81 ^b	100	0
2	Ag _{0.2} Pd _{0.8}	41	123 ^b	100	0
3	Ag _{0.5} Pd _{0.5}	67	201 ^b	100	0
4	Ag _{0.8} Pd _{0.2}	35	105 ^b	100	0
5	Ag	20	60 ^b	100	0
6	(CuO) _{0.2} Pd _{0.8}	15	11 ^c	100	0
7	(CuO) _{0.5} Pd _{0.5}	5.9	5.9 ^c	100	0
8	(CuO) _{0.8} Pd _{0.2}	3.3	7.6 ^c	100	0
9	CuO/Cu ₂ O	0.8	-	100	0

[a] Reaction conditions: styrene (3 mmol), NP-IL (0.05 mL), IL (0.45 mL), H₂ (2 MPa), 353 K, 1 h (IL = [C₂OHmim][NTf₂]). [b] activity = moles of converted substrate/moles of Ag and Pd. [c] activity = moles of converted substrate/moles of Pd.

Table 5. Hydrogenation of 4-bromotoluene catalysed by Ag, Pd, CuO, Ag-Pd and CuO-Pd NPs in [C₂OHmim][NTf₂].^a

Entry	NPs	Conversion [%]	Activity [h ⁻¹]	Selectivity for toluene [%]	Selectivity for 1-bromo-4-methylcyclohexane [%]
1	Pd	36	18	100	0
2	Ag _{0.2} Pd _{0.8}	60	37	100	0
3	Ag _{0.5} Pd _{0.5}	42	42	100	0
4	Ag _{0.8} Pd _{0.2}	23	58	100	0
5	Ag	0	-	-	-
6	(CuO) _{0.2} Pd _{0.8}	9.9	7.2	100	0
7	(CuO) _{0.5} Pd _{0.5}	1.2	1.2	100	0
8	(CuO) _{0.8} Pd _{0.2}	1.1	2.5	100	0
9	CuO/Cu ₂ O	0	-	-	-

[a] Reaction conditions: 4-bromotoluene (0.5 mmol), NP-IL (0.05 mL), IL (0.5 mL), K₂CO₃ (0.069 g), H₂ (3 MPa), 343 K, 2 h (IL = [C₂OHmim][NTf₂]). [b] activity = moles of converted substrate/moles of Pd

Synthesis and Characterization of CuO-Pd NPs

Following a similar protocol as described above for AgPd NPs, thermal decomposition of Pd(OAc)₂ and Cu(OAc)₂ (with Pd:Cu ratio of 10:0, 8:2, 5:5, 2:8 and 0:10) was carried out in [C₂OHmim][NTf₂]. The resulting NPs were systematically investigated with ICP-OES, TEM, XRD and XPS analysis. Since previous reports claimed that the decomposed products of either Cu(OAc)₂ or Cu(OAc)₂·H₂O contained a large percentage of CuO_x,⁸⁷⁻⁸⁹ the presence of Cu or CuO was finely studied. Interestingly, the NPs containing Cu and Pd are drastically different from Ag-Pd NPs prepared by the same method, in terms of both metal valence state and NP structure.

As presented in Figure 4, TEM images showed that the Cu-based NPs are well dispersed with a mean size of ca. 3.9 nm, whereas the size of bimetallic CuO-Pd NPs is estimated to be in the range 7-10 nm. The elemental ratio of total CuO-Pd NPs calculated based on ICP-OES analysis and the surface composition calculated using XPS analysis are given in Table 6. It is clear that the near surface Cu:Pd is much larger than the total elemental ratio of Cu:Pd in NPs, which implies that the

Cu-Pd NPs may also adopt a core-shell type structure, with Pd atoms in the core.

ICP-OES result in Table 6 showed that the Cu to Pd ratio has some derivation from the stoichiometric ratio of Cu and Pd reacted precursors. Nonetheless, the trend is clear that with increasing amount of Cu precursor, the Cu content in the resulting NPs increases accordingly. XPS was employed to investigate the electronic state of Cu and Pd in the NPs. As can be seen in Figure 5 (b), the satellite peak of Cu(II) at around 943.5 eV exists for all the NPs.⁹⁰ Based on the ICP result that most of the precursor has been consumed, the Cu(II) should be attributed to CuO, which is later confirmed by XRD analysis. In Figure 5 (b), two sets of binding energy of the Cu 2p electrons were obtained for NPs prepared from Cu(OAc)₂. The lower one (around 931.3 eV) may correspond to Cu₂O or even Cu, while the larger one (around 933.4 eV) can be assigned to CuO. The two types of Cu species have a 2:3 ratio. Auger spectra (Figure 6) were employed to further clarify the electronic state of the unknown Cu species. The kinetic energy obtained from Figure 6a is 916.8 eV, close to that of Cu₂O standard (916.2-917.2 eV).⁹¹ Then the Auger parameter and Wagner plots were employed to confirm the existence of Cu(I).⁹² Further, Auger Cu LMM spectra (Figure 6b) corroborates the coexistence of Cu⁺ at BE ca. 569.6 eV and Cu²⁺ at BE ca. 568.5 eV.⁹³ For the other three NP samples, only a peak corresponding to CuO was detected, suggesting CuO is the predominant Cu species on the surface. In Figure 5 (a), the binding energy of Pd 3d_{5/2} electron stayed at 335.1 -335.4 eV (corresponding to metallic Pd) regardless of CuO content. As such, the NPs appear to be a metal-metal oxide nanocomposite, consisting of CuO and Pd. A close inspection of the XPS spectra indicates that the binding energy of Cu increases with more Pd incorporation while the tendency is the reverse for Pd. Therefore, charge transfer occurred from Cu to Pd in the CuO-Pd NPs. The valence state of the CuO-Pd NPs obtained here appears different from that observed for colloids formed by thermal decomposition of the two acetates in some organic solvents, namely Cu-Pd and Cu₂O-Pd.⁸⁷ Such a difference may be due to the fact that the hydroxyl-functionalized ionic liquid employed in this study has a high affinity for water, which can facilitate the formation of oxide during the decomposition process. Decomposition of Cu(OAc)₂·H₂O in an imidazole-based ionic liquid [C₄mim][OAc] was also studied and a mixture of Cu₂O and CuO was obtained.⁸⁹

XRD was employed to determine the crystalline structure of the NPs. As shown in Figure 7, only reflections for CuO (peaks centred at 36° and 38°) were found for the NP sample obtained from decomposition of Cu(OAc)₂, in agreement with XPS analysis.

The XRD patterns of both (CuO)_{0.2}Pd_{0.8} and (CuO)_{0.5}Pd_{0.5} bimetallic NPs show only four predominant peaks centred at 40°, 47°, 68° and 82°, matching the characteristic (111), (200), (300) and (220) reflections of Pd (0), while no crystalline domains of CuO_x or Cu were observed. This phenomenon further corroborates that the structure of these NPs is a palladium core covered by a CuO enriched shell, which could

be expected as copper is more oxophilic and thus will be attracted outside in presence of oxygen atoms of the hydroxyl groups.^{94,95} For $(\text{CuO})_{0.8}\text{Pd}_{0.2}$ NPs, the diffraction peaks for Pd (0) were not observed, which may be due to the fact that CuO

NPs corroborates with the structural features of these NPs, i.e., the catalytically active Pd is mostly buried inside the particle.

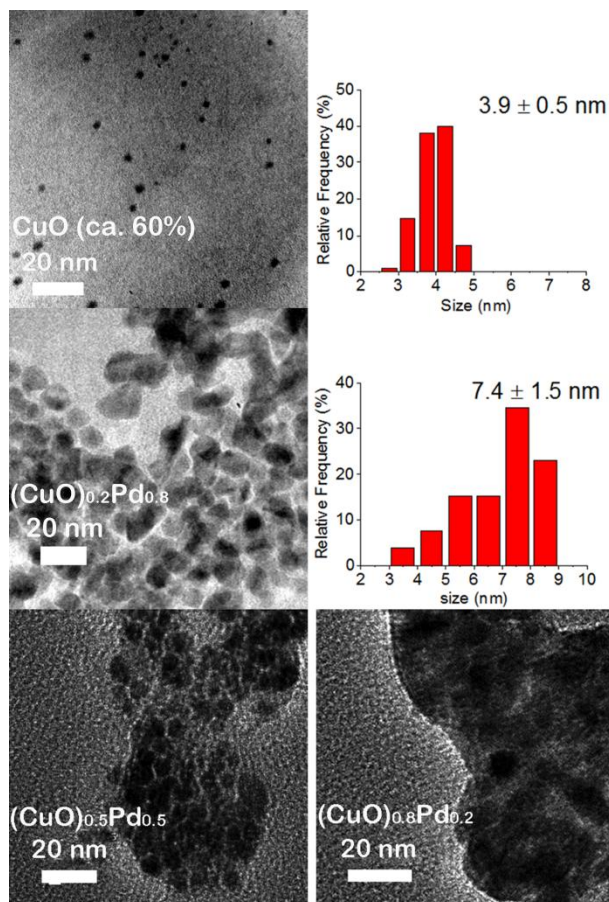


Figure 4. TEM images and size distribution of CuO-Pd NPs (the NPs $(\text{CuO})_{0.5}\text{Pd}_{0.5}$ and $(\text{CuO})_{0.8}\text{Pd}_{0.2}$ are not well separated, therefore their size distribution is not provided)

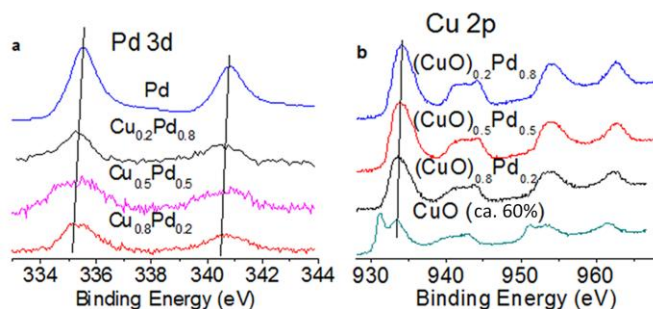


Figure 5. XPS spectra of Pd 3d peak (a) and Cu 2p peak (b) for CuO-Pd NPs.

takes up most of the NPs and the crystalline size of Pd core is too small to be detected by XRD. The four reactions to evaluate Ag-Pd NPs were conducted under the same conditions over these CuO-Pd NPs (Tables 2-5, Entries 6-9). The CuO-Pd NPs are more active than pure CuO NPs but much less active than pure Pd NPs in all cases. The catalytic performance of CuO-Pd

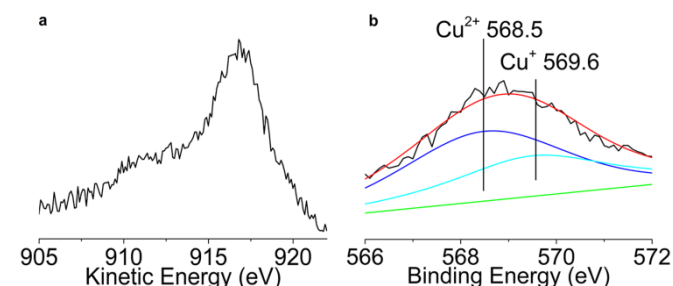


Figure 6 Cu KLL (a) and Cu LMM (b) XP spectra of the decomposed products of $\text{Cu}(\text{OAc})_2$

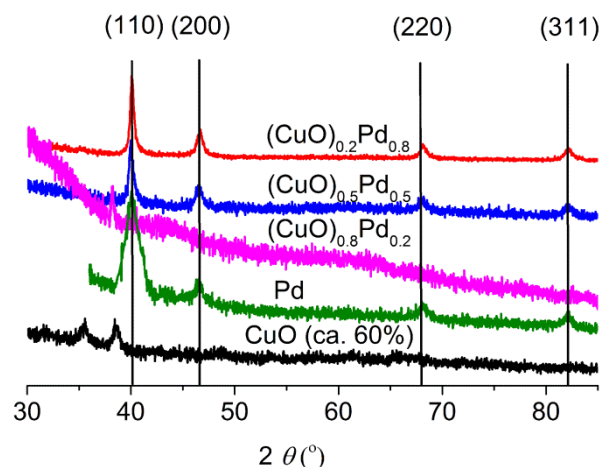


Figure 7. X-ray diffraction patterns of CuO-Pd NPs. The predicted diffraction peaks for CuO and Pd metal are indicated. From top to bottom: $(\text{CuO})_{0.2}\text{Pd}_{0.8}$, $(\text{CuO})_{0.5}\text{Pd}_{0.5}$, $(\text{CuO})_{0.8}\text{Pd}_{0.2}$, Pd and CuO.

Table 6. Elemental composition of CuO-Pd NPs calculated from ICP analysis and the surface composition calculated from XPS analysis

NPs ^a	Cu/Pd ratio	Surface Cu/Pd ratio
CuO-Pd (4:1)	2:1	7.52:1
CuO-Pd (1:1)	0.74:1	7.38:1
CuO-Pd (0.25:1)	0.22:1	1.42:1

[a] This ratio corresponds to the initial molar amount of two acetates.

Experimental

Materials and methods

Materials were purchased as following: Palladium (II) acetate (Pd 48%), copper (II) acetate (Cu 34%), silver acetate ($\geq 99.0\%$) from Sinopharm Chemical Reagent; $[\text{C}_2\text{OH}][\text{NTf}_2]$ from Centre for Green Chemistry and Catalysis, Lanzhou Institute of Chemical Physics, Chinese Academy of Science; Ethyl acetate (AR) from Merck Pte Ltd.; Acetonitrile from Tedia.com. inc.; Ethanol (analytical reagent grade) and diethyl ether (analytical reagent grade) from Fisher Scientific UK; Styrene ($\geq 99\%$), nitrobenzene (99%), 4-nitrophenol (\geq

99.5%), 4-bromotoluene (98%) and cyclohexanone ($\geq 99.0\%$) from Sigma Aldrich.

ICP analysis

Metal content in Ag-Pd NP series was determined by iCAP 6000 series inductively coupled plasma optical emission spectrometry (ICP-OES). For Cu-Pd NPs it was determined by Agilent Technologies 7500 series inductively coupled plasma mass spectrometry (ICP-MS). Both the NPs and the supernatants obtained from purification step were analysed. The supernatant was transferred to another flask whereas all the NPs were re-dispersed in acetonitrile (2 ml, solution A). 1/4 of the total volume of the solution A and 1/3 of supernatants (both were treated with rotary evaporator to remove the solvents before dissolving) were digested in aqua regia (8 mL, HCl/HNO₃ = 3:1) at 353 K for 4 h and then diluted with deionized water to 100 mL before analysis.

TEM

Transmission electron microscopy (TEM) measurements were carried out with JEOL JEM-2010 electron microscope operated at 200 kV. After isolation by centrifugation (*vide infra*), the NPs were re-dispersed in acetonitrile and sonicated for 5 seconds. One drop of the NP solution was placed onto a copper grid coated with carbon film and dried over night at room temperature (r.t.). The average diameter of the NPs was determined through analysis of 150-200 NPs with Adobe Acrobat 9 Pro.

XRD

X-ray diffraction (XRD) analysis was carried out using a Bruker D8 Advance X-Ray Diffractometer with Cu K α radiation, at a scan rate of 8°/min with scanning angle from 30° to 85° (Pd from 36° to 85°). It was operated at 40 kV applying a potential current of 30 mA.

XPS

X-ray photoelectron spectroscopy (XPS) was performed under Al K α radiation ($h\nu = 1486.71$ eV) at 5×10^{-9} Torr. The Model is Kratos AXIS Ultra DLD. Binding energies (BE) are calibrated by the C (1s) binding energy of adventitious carbon contamination (set at 284.6 eV). The analysis of Pd, Ag and Cu was based on Pd 3d, Ag 3d and Cu 2p peaks, respectively.

GC

For all catalytic reactions, an Agilent 7890A gas chromatography (GC) system equipped with a flame ionization detector and a HP-5 capillary column was employed following the internal standard method to determine reactivity (conversion and selectivity).

Preparation of the bimetallic NPs

The synthetic procedure applied for preparing Ag_{0.5}Pd_{0.5} NPs is given as a typical experiment : Pd(OAc)₂ (11.2 mg, 0.05 mmol) and Ag(OAc) (8.3 mg, 0.05 mmol) were dissolved in

acetonitrile (4 mL) under vigorous stirring and then mixed with [C₂OHmim][NTf₂] (1 mL) in a round bottom flask (10 mL) covered with an aluminium foil. The acetonitrile was evaporated under vacuum at 310 K for 30 min. Kept under vacuum (to remove of the volatile compounds during the decompenation), the system was heated at 393 K in a pre-heated oil bath for 2 h with intensive stirring (800 r/min), during which co-decomposition of Pd(OAc)₂ and Ag(OAc) occurred, affording a dark brown colloidal suspension. After cooling to r.t., two different post treatment methods were performed for characterization.

For XRD and XPS analysis, the NP/IL suspension was centrifuged at 8000 r/min for 4 min. The supernatant was removed and the remaining NPs were collected for measurement.

For ICP-OES and TEM analysis, the colloidal suspension was diluted with acetone/ethanol (10 mL in total, v/v=7:3). Then the organic phase and the NPs were separated through centrifugation (8400 r/min, 4 min) at r.t.. Staying at the bottom, the NPs were easily separated whereas the supernatant contained a mixture of washing solvent, IL and unreacted precursors.

Pd NPs suspension was treated in the same way, except that the suspension was diluted with ethanol/water (10 mL in total, v/v=7:3) instead of acetone/ethanol for easier separation.

For the synthesis of CuO and CuO-Pd NPs, the procedure was slightly modified. 413 K was selected as temperature decomposition without using an aluminium foil. After cooling down at r.t., a mixture of ethanol/water (10 ml in total, v/v=7:3) was added to the suspension of NPs for their isolation by centrifugation after adding.

Catalytic reactions with Ag-Pd and CuO-Pd bimetallic NPs

Hydrogenation of 4-nitrophenol: The substrate (70 mg, 0.5 mmol), NP/IL suspension (0.05 mL), IL (0.45 mL) and K₂CO₃ (50 mg, 0.36 mmol) were introduced into an autoclave. The reaction was performed at 353 K under H₂ (3.0 MPa) for 2 h. Reaction products were extracted with ethyl acetate (5 mL) in the autoclave for 30 min (800 r/min) and analyzed by GC.

Hydrogenation of nitrobenzene: The substrate (0.10 mL, 1.0 mmol), NP/IL suspension (0.05 mL), IL (0.45 mL) were added into an autoclave. The reaction was performed at 333 K under H₂ (2.0 MPa) for 2 h. Reaction products were extracted with diethyl ether (5 mL) and analyzed by GC.

Hydrogenation of styrene: The substrate (0.345 mL, 3.0 mmol), NP/IL suspension (0.05 mL), IL (0.45 mL) were added into an autoclave. The reaction was performed at 333 K under H₂ (2.0 MPa) for 1 h. Reaction products were extracted with diethyl ether (5 mL) and analyzed by GC.

Dehalogenation of 4-bromotoluene: The substrate (85.5 mg, 0.5 mmol), NP/IL suspension (0.05 mL), IL (0.5 mL), K₂CO₃ (69 mg, 0.5 mmol) were added into an autoclave. The reaction was performed at 343 K under H₂ (3.0 MPa) for 2 h. Reaction products were extracted by ethyl acetate (5 mL) and analyzed by GC.

Conclusions

Ag-Pd and CuO-Pd NPs were easily obtained through thermal decomposition under vacuum of corresponding acetate salts in [C₂OHmim][NTf₂]. The composition of these NPs could be adjusted by changing the ratio of the two precursors. Both the Ag and Pd in the Ag-Pd NPs are in the metallic state, adapting a core-shell structure with Ag in the inner part and Pd in the outer layer. Charge transfer from Pd to Ag was observed by XPS, which endows the NPs with special electrical properties and promotes their catalytic performance in hydrogenation. For the CuO-Pd NPs, Pd has a high tendency to stay in the core while CuO prefers to be located on the surface, as expected given its oxophilic character. This study enlightens that thermal decomposition of metal acetates is a convenient method to prepare various bimetallic NPs in ILs with core-shell structure, for applications in catalysis and potentially beyond.

Acknowledgements

The authors thank the A*Star, PSF funding (WBS: R-279-000-403-305), the Merlion project (WBS: R-279-000-421-133) and CNRS for financial support.

Notes and references

a Department of Chemical and Biomolecular Engineering, National University of Singapore, 4 Engineering Drive 4, Singapore .

b Laboratoire de Chimie de Coordination, CNRS, BP 44099, 205 Route de Narbonne, F-31077 Toulouse Cedex 4, France .

c Université de Toulouse, UPS, INPT, LCC, F-31077 Toulouse, France.

E-mail: ning.yan@nus.edu.sg

- (1) Moskovits, M.; Srnov & Šloufová, I.; Vlčková, B. *J. Chem. Phys.* **2002**, *116*, 10435.
- (2) Toshima, N.; Kanemaru, M.; Shiraishi, Y.; Koga, Y. *J. Phys. Chem. B* **2005**, *109*, 16326.
- (3) Park, J. Y.; Zhang, Y.; Grass, M.; Zhang, T.; Somorjai, G. A. *Nano Lett.* **2008**, *8*, 673.
- (4) Yan, N.; Xiao, C.; Kou, Y. *Coord. Chem. Rev.* **2010**, *254*, 1179.
- (5) Toshima, N.; Yonezawa, T. *New J. Chem.* **1998**, *22*, 1179.
- (6) Liu, X.; Liu, X. *Angew. Chem. Int. Ed.* **2012**, *51*, 3311.
- (7) Huang, X.; Zhang, H.; Guo, C.; Zhou, Z.; Zheng, N. *Angew. Chem.* **2009**, *121*, 4902.
- (8) Senapati, S.; Ahmad, A.; Khan, M. I.; Sastry, M.; Kumar, R. *Small* **2005**, *1*, 517.
- (9) Gu, H.; Yang, Z.; Gao, J.; Chang, C. K.; Xu, B. *J. Am. Chem. Soc.* **2004**, *127*, 34.
- (10) Serpell, C. J.; Cookson, J.; Ozkaya, D.; Beer, P. D. *Nat. Chem.* **2011**, *3*, 478.
- (11) Ghosh Chaudhuri, R.; Paria, S. *Chem. Rev.* **2011**, *112*, 2373.
- (12) Park, J. H.; Chung, Y. K. *Dalton Trans.* **2008**, 2369.
- (13) Alayoglu, S.; Nilekar, A. U.; Mavrikakis, M.; Eichhorn, B. *Nat. Mater.* **2008**, *7*, 333.
- (14) Edwards, J. K.; Hutchings, G. J. *Angew. Chem. Int. Ed.* **2008**, *47*, 9192.
- (15) Schmid, G.; West, H.; Mehles, H.; Lehnert, A. *Inorg. Chem.* **1997**, *36*, 891.
- (16) Alayoglu, S.; Eichhorn, B. *J. Am. Chem. Soc.* **2008**, *130*, 17479.
- (17) Lee, Y. W.; Kim, M.; Kim, Z. H.; Han, S. W. *J. Am. Chem. Soc.* **2009**, *131*, 17036.
- (18) Jose, D.; Jagirdar, B. R. *J. Phys. Chem. C* **2008**, *112*, 10089.
- (19) Lu, C.-L.; Prasad, K. S.; Wu, H.-L.; Ho, J.-a. A.; Huang, M. H. *J. Am. Chem. Soc.* **2010**, *132*, 14546.
- (20) Mandal, S.; Selvakannan, P. R.; Pasricha, R.; Sastry, M. *J. Am. Chem. Soc.* **2003**, *125*, 8440.
- (21) Jiang, H.-L.; Akita, T.; Ishida, T.; Haruta, M.; Xu, Q. *J. Am. Chem. Soc.* **2011**, *133*, 1304.
- (22) Joo, S. H.; Park, J. Y.; Tsung, C.-K.; Yamada, Y.; Yang, P.; Somorjai, G. A. *Nat. Mater.* **2009**, *8*, 126.
- (23) Alayoglu, S.; Zavalij, P.; Eichhorn, B.; Wang, Q.; Frenkel, A. I.; Chupas, P. *ACS Nano* **2009**, *3*, 3127.
- (24) Lara, P.; Casanove, M.-J.; Lecante, P.; Fazzini, P.-F.; Philippot, K.; Chaudret, B. *J. Mater. Chem.* **2012**, *22*, 3578.
- (25) Lara, P.; Ayval, T.; Casanove, M.-J.; Lecante, P.; Mayoral, A.; Fazzini, P.-F.; Philippot, K.; Chaudret, B. *Dalton Trans.* **2013**, *42*, 372.
- (26) Lim, B.; Wang, J.; Camargo, P. H. C.; Jiang, M.; Kim, M. J.; Xia, Y. *Nano Lett.* **2008**, *8*, 2535.
- (27) Kobayashi, H.; Yamauchi, M.; Kitagawa, H.; Kubota, Y.; Kato, K.; Takata, M. *J. Am. Chem. Soc.* **2008**, *130*, 1818.
- (28) Kobayashi, H.; Yamauchi, M.; Kitagawa, H.; Kubota, Y.; Kato, K.; Takata, M. *J. Am. Chem. Soc.* **2010**, *132*, 5576.
- (29) Zhang, J.; Asakura, H.; van Rijn, J.; Yang, J.; Duchesne, P.; Zhang, B.; Chen, X.; Zhang, P.; Saeys, M.; Yan, N. *Green Chem.* **2014**, *16*, 2432.
- (30) Zhang, J.; Teo, J.; Chen, X.; Asakura, H.; Tanaka, T.; Teramura, K.; Yan, N. *ACS Catal.* **2014**, *4*, 1574.
- (31) Dupont, J.; Fonseca, G. S.; Umpierre, A. P.; Fichtner, P. F. P.; Teixeira, S. R. *J. Am. Chem. Soc.* **2002**, *124*, 4228.
- (32) Precht, M. H. G.; Scariot, M.; Scholten, J. D.; Machado, G.; Teixeira, S. R.; Dupont, J. *Inorg. Chem.* **2008**, *47*, 8995.
- (33) L'éger, B.; Denicourt-Nowicki, A.; Olivier-Bourbigou, H.; Roucoux, A. *Tetrahedron Lett.* **2009**, *50*, 6531.
- (34) Precht, M. H. G.; Campbell, P. S.; Scholten, J. D.; Fraser, G. B.; Machado, G.; Santini, C. C.; Dupont, J.; Chauvin, Y. *Nanoscale* **2010**, *2*, 2601.
- (35) Denicourt-Nowicki, A.; Leger, B.; Roucoux, A. *Phys. Chem. Chem. Phys.* **2011**, *13*, 13510.
- (36) Banerjee, A.; Theron, R.; Scott, R. W. *J. ChemSusChem* **2012**, *5*, 109.
- (37) Dupont, J.; Scholten, J. D. *Chem. Soc. Rev.* **2010**, *39*, 1780.
- (38) Ott, L. S.; Cline, M. L.; Deetlefs, M.; Seddon, K. R.; Finke, R. G. *J. Am. Chem. Soc.* **2005**, *127*, 5758.
- (39) Zhang, B.; Yan, N. *Catalysts* **2013**, *3*, 543.
- (40) Yang, X.; Yan, N.; Fei, Z.; Crespo-Quesada, R. M.; Laurency, G.; Kiwi-Minsker, L.; Kou, Y.; Li, Y.; Dyson, P. J. *Inorg. Chem.* **2008**, *47*, 7444.
- (41) Sun, J.; Zhang, S.; Cheng, W.; Ren, J. *Tetrahedron Lett.* **2008**, *49*, 3588.
- (42) Darwich, W.; Gedig, C.; Srour, H.; Santini, C. C.; Precht, M. H. G. *RSC Adv.* **2013**, *3*, 20324.

- (43) Zhao, D.; Fei, Z.; Geldbach, T. J.; Scopelliti, R.; Dyson, P. J. *J. Am. Chem. Soc.* **2004**, *126*, 15876.
- (44) Zhang, Q.; Li, Z.; Zhang, J.; Zhang, S.; Zhu, L.; Yang, J.; Zhang, X.; Deng, Y. *J. Phys. Chem. B* **2007**, *111*, 2864.
- (45) Kim, K.-S.; Dembereinyamba, D.; Lee, H. *Langmuir* **2003**, *20*, 556.
- (46) Tatumi, R.; Fujihara, H. *Chem. Commun.* **2005**, 83.
- (47) Nockemann, P.; Thijs, B.; Parac-Vogt, T. N.; Van Hecke, K.; Van Meerelt, L.; Tinant, B.; Hartenbach, I.; Schleid, T.; Ngan, V. T.; Nguyen, M. T.; Binnemans, K. *Inorg. Chem.* **2008**, *47*, 9987.
- (48) Zhang, H.; Cui, H. *Langmuir* **2009**, *25*, 2604.
- (49) Fei, Z.; Zhao, D.; Pieraccini, D.; Ang, W. H.; Geldbach, T. J.; Scopelliti, R.; Chiappe, C.; Dyson, P. J. *Organometallics* **2007**, *26*, 1588.
- (50) Yan, N.; Yuan, Y.; Dyson, P. J. *Dalton Trans.* **2013**, *42*, 13294.
- (51) Yuan, Y.; Yan, N.; Dyson, P. J. *ACS Catal.* **2012**, *2*, 1057.
- (52) Siankevich, S.; Savoglidis, G.; Fei, Z.; Laurencyzy, G.; Alexander, D. T. L.; Yan, N.; Dyson, P. J. *J. Catal.* **2014**, *315*, 67.
- (53) Dash, P.; Dehm, N. A.; Scott, R. W. J. *J. Mol. Catal. A: Chem.* **2008**, *286*, 114.
- (54) Okazaki, K.-i.; Kiyama, T.; Hirahara, K.; Tanaka, N.; Kuwabata, S.; Torimoto, T. *Chem. Commun.* **2008**, 691.
- (55) Tsai, T.-H.; Thiagarajan, S.; Chen, S.-M. *J. Appl. Electrochem.* **2010**, *40*, 493.
- (56) Xiao, F.; Mo, Z.; Zhao, F.; Zeng, B. *Electrochem. Commun.* **2008**, *10*, 1740.
- (57) Zhang, G.; Zhou, H.; An, C.; Liu, D.; Huang, Z.; Kuang, Y. *Colloid. Polym. Sci.* **2012**, *290*, 1435.
- (58) Wang, Y.; Yang, H. *J. Am. Chem. Soc.* **2005**, *127*, 5316.
- (59) Xiao, F.; Zhao, F.; Mei, D.; Mo, Z.; Zeng, B. *Biosens. Bioelectron.* **2009**, *24*, 3481.
- (60) Xue, X.; Lu, T.; Liu, C.; Xu, W.; Su, Y.; Lv, Y.; Xing, W. *Electrochim. Acta* **2005**, *50*, 3470.
- (61) Jiang, T.; Zhou, Y.; Liang, S.; Liu, H.; Han, B. *Green Chem.* **2009**, *11*, 1000.
- (62) Ding, K.; Yang, H.; Cao, Y.; Zheng, C.; Rapole, S. B.; Guo, Z. *Mater. Chem. Phys.* **2013**, *142*, 403.
- (63) Yuan, X.; Sun, G.; Asakura, H.; Tanaka, T.; Chen, X.; Yuan, Y.; Laurencyzy, G.; Kou, Y.; Dyson, P. J.; Yan, N. *Chem. Eur. J.* **2013**, *19*, 1227.
- (64) Yuan, X.; Yan, N.; Katsyuba, S. A.; Zvereva, E. E.; Kou, Y.; Dyson, P. J. *Phys. Chem. Chem. Phys.* **2012**, *14*, 6026.
- (65) Gutel, T.; Garcia-Anton, J.; Pelzer, K.; Philippot, K.; Santini, C. C.; Chauvin, Y.; Chaudret, B.; Basset, J.-M. *J. Mater. Chem.* **2007**, *17*, 3290.
- (66) Pelzer, K.; Vidoni, O.; Philippot, K.; Chaudret, B.; Collière, V. *Adv. Funct. Mater.* **2003**, *13*, 118.
- (67) Dash, P.; Scott, R. W. J. *Chem. Commun.* **2009**, 812.
- (68) Bell, W. C.; Myrick, M. L. *J. Colloid Interf. Sci.* **2001**, *242*, 300.
- (69) Itoh, H.; Naka, K.; Chujo, Y. *J. Am. Chem. Soc.* **2004**, *126*, 3026.
- (70) Anastas, P.; Eghbali, N. *Chem. Soc. Rev.* **2010**, *39*, 301.
- (71) Koh, S.; Strasser, P. *J. Am. Chem. Soc.* **2007**, *129*, 12624.
- (72) Tai, C.-C.; Su, F.-Y.; Sun, I. W. *Electrochim. Acta* **2005**, *50*, 5504.
- (73) Safavi, A.; Momeni, S.; Tohidi, M. *Electroanal.* **2012**, *24*, 1981.
- (74) Safavi, A.; Kazemi, H.; Momeni, S.; Tohidi, M.; Khanipour Mehrin, P. *Int. J. Hydrogen Energy* **2013**, *38*, 3380.
- (75) He, J.; Ichinose, I.; Kunitake, T.; Nakao, A.; Shiraishi, Y.; Toshima, N. *J. Am. Chem. Soc.* **2003**, *125*, 11034.
- (76) Liu, J.; Zhou, H.; Wang, Q.; Zeng, F.; Kuang, Y. *J. Mater. Sci.* **2012**, *47*, 2188.
- (77) Wei, H.-H.; Yen, C. H.; Lin, H.-W.; Tan, C.-S. *J. Supercrit. Fluids* **2013**, *81*, 1.
- (78) Lu, Y.; Chen, W. *J. Phys. Chem. C* **2010**, *114*, 21190.
- (79) Li, N.; Wang, W.; Tian, D.; Cui, H. *Chem. Commun.* **2010**, *46*, 1520.
- (80) Tang, S.; Vongehr, S.; Zheng, Z.; Liu, H.; Meng, X. *J. Phys. Chem. C* **2010**, *114*, 18338.
- (81) Slanac, D. A.; Hardin, W. G.; Johnston, K. P.; Stevenson, K. J. *J. Am. Chem. Soc.* **2012**, *134*, 9812.
- (82) Kitchin, J. R.; Reuter, K.; Scheffler, M. *Phys. Rev. B: Condens. Matter* **2008**, *77*, 075437.
- (83) Wen, H.; Yao, K.; Zhang, Y.; Zhou, Z.; Kirschning, A. *Catal. Commun.* **2009**, *10*, 1207.
- (84) Li, J.; Shi, X.-Y.; Bi, Y.-Y.; Wei, J.-F.; Chen, Z.-G. *ACS Catal.* **2011**, *1*, 657.
- (85) Cárdenas-Lizana, F.; de Pedro, Z. M.; Gómez-Quero, S.; Keane, M. A. *J. Mol. Catal. A: Chem.* **2010**, *326*, 48.
- (86) Liu, H.; Jiang, T.; Han, B.; Liang, S.; Zhou, Y. *Science* **2009**, *326*, 1250.
- (87) Esumi, K.; Tano, T.; Torigoe, K.; Meguro, K. *Chem. Mater.* **1990**, *2*, 564.
- (88) Judd, M. D.; Plunkett, B. A.; Pope, M. I. *J. Therm. Anal.* **1974**, *6*, 555.
- (89) Swadzba-Kwasny, M.; Chancelier, L.; Ng, S.; Manyar, H. G.; Hardacre, C.; Nockemann, P. *Dalton Trans.* **2012**, *41*, 219.
- (90) Lee, S. Y.; Mettlach, N.; Nguyen, N.; Sun, Y. M.; White, J. M. *Appl. Surf. Sci.* **2003**, *206*, 102.
- (91) Molder, J.; Sickel, W.; Sobol, P.; Bomben, K. *Handbook of X-ray Photoelectron Spectroscopy*, 1992.
- (92) Moretti, G. *J. Electron. Spectrosc. Relat. Phenom.* **1998**, *95*, 95.
- (93) Liu, P.; Hensen, E. J. M. *J. Am. Chem. Soc.* **2013**, *135*, 14032.
- (94) Kern, D. M. H. *J. Am. Chem. Soc.* **1953**, *75*, 2473.
- (95) Zuo, Y.; Tang, J.; Fan, C.; Tang, Y.; Xiong, J. *Thin Solid Films* **2008**, *516*, 7565.